Apical constriction and invagination downstream of the canonical Wnt signaling pathway requires Rho1 and Myosin II

Sandra G. Zimmerman, **Lauren M. Thorpe**, **Vilma R. Medrano**, **Carolyn A. Mallozzi**, and **Brooke M. McCartney**[*]

Department of Biological Sciences, Carnegie Mellon University, 4400 5th Avenue, Pittsburgh, PA 15213, USA

Abstract

The tumor suppressor Adenomatous polyposis coli (APC) is a negative regulator of Wnt signaling and functions in cytoskeletal organization. Disruption of human APC in colonic epithelia initiates benign polyps that progress to carcinoma following additional mutations. The early events of polyposis are poorly understood, as is the role of canonical Wnt signaling in normal epithelial architecture and morphogenesis. To determine the consequences of complete loss of APC in a model epithelium, we generated *APC2 APC1* double null clones in the *Drosophila* wing imaginal disc. APC loss leads to segregation, apical constriction, and invagination that result from transcriptional activation of canonical Wnt signaling. Further, we show that Wnt-dependent changes in cell fate can be decoupled from Wnt-dependent changes in cell shape. Wnt activation is reported to upregulate *DE-cadherin* in wing discs, and elevated DE-cadherin is thought to promote apical constriction. We find that apical constriction and invagination of *APC* null tissue are independent of DE-cadherin elevation, but are dependent on Myosin II activity. Further, we show that disruption of Rho1 suppresses apical constriction and invagination in *APC* null cells. Our data suggest a novel link between canonical Wnt signaling and epithelial structure that requires activation of the Rho1 pathway and Myosin II.

Keywords

Wnt; morphogenesis; Adenomatous Polyposis Coli; *Drosophila*; imaginal disc; apical constriction

Introduction

The canonical Wnt pathway is negatively regulated by the destruction complex, which includes GSK3β, Axin, and the colon cancer tumor suppressor Adenomatous polyposis coli (APC) (van Amerongen and Nusse, 2009). The destruction complex targets cytoplasmic β-

[*]Corresponding Author. Brooke M. McCartney, Department of Biological Sciences, Carnegie Mellon University, 4400 5th Avenue, Pittsburgh, PA 15213, USA, bmccartney@cmu.edu, +1-412-268-5195.

catenin (β-cat)/Armadillo (Arm, *Drosophila* β-catenin) for ubiquitination and degradation by the proteosome. In the presence of Wnt, the destruction complex is deactivated, and stabilized β-cat/Arm enters the nucleus where it activates Wnt target genes together with the transcriptional activator TCF. In addition to its well-known roles in establishing cell fate and promoting proliferation during animal development (Cadigan and Nusse, 1997; Couso et al., 1994; Neumann and Cohen, 1996; Neumann and Cohen, 1997; Struhl and Basler, 1993), changes in canonical Wnt signaling are associated with a variety of cancers (reviewed in Reya and Clevers, 2005). Loss of function mutations in *APC* result in the inappropriate activation of Wnt target genes, initiating benign colon polyps and the development of colon cancer (reviewed in Reya and Clevers, 2005). Further, studies suggest that *APC* mutations may contribute to tumorigenesis not only by activating the canonical Wnt pathway but also by directly affecting the cytoskeleton (reviewed in McCartney and Nathke, 2008). APC influences dynamic instability and promotes microtubule stability (Kita et al., 2006; Kroboth et al., 2007; Wen et al., 2004), promotes microtubule-kinetochore interactions (Green and Kaplan, 2003), and acts as part of a "cortical template" that organizes microtubule networks (Reilein and Nelson, 2005). Furthermore, vertebrate APC interacts with the RacGEF ASEF and IQGAP, an effector of Rac1 and Cdc42 to influence actin (Kawasaki et al., 2000; Watanabe et al., 2004). Drosophila APC2, together with the formin Diaphanous, was recently shown to promote actin furrow extension in the Drosophila syncytial embryo (Webb et al., 2009). Early polyposis in the mouse intestine is characterized by an apparent invagination of *APC* mutant cells (Cortina et al., 2007; Oshima et al., 1997 and Supplementary Fig. 6C–E), suggesting that disruption of APC in the mammalian intestinal epithelium affects tissue morphology. However, the precise cellular changes driving that invagination, and the molecular requirements for those changes, are not well understood. While the non-canonical Wnt planar cell polarity pathway has well-described roles in tissue morphogenesis, the role of the canonical pathway is not well known.

To examine the effects of complete loss of APC and activation of Wnt signaling on epithelial morphology, we generated tissue mutant for both *Drosophila APC* genes, *APC2* and *APC1*, in the larval wing imaginal disc. The wing disc (the adult wing primordium) is an epithelial sac (Supplementary Fig. 1A). One side of the sac is the "disc proper", and at the late 3rd instar consists primarily of a single layer of polarized, pseudostratified, columnar epithelial cells that is folded in a highly stereotyped manner. The disc proper develops into the wing blade, hinge, notum, and ventral pleura. The other side of the sac is primarily a squamous epithelium (peripodial epithelium) that is required for patterning of the disc proper and contributes to some adult structures (reviewed in Gibson and Schubiger, 2001; McClure and Schubiger, 2005). During the late third instar, Wingless (*Drosophila* Wnt-1) is expressed in a stripe at the dorsal-ventral D/V boundary and is required for wing margin specification (Couso et al., 1994). Expression in two rings around the wing pouch, and in a broad stripe across the notum, has been fate mapped to the hinge (Casares and Mann, 2000; Neumann and Cohen, 1996)

Here we show that complete loss of *APC2* and *APC1* in clones in the wing imaginal epithelium results in canonical Wnt-dependent cell segregation, apical constriction, and invagination that do not require Wnt-dependent changes in final cell fate. Our evidence

suggests a novel link between canonical Wnt signaling and epithelial morphology that requires Rho1 and Myosin II.

Materials and methods

Fly Stocks and Genetics

Fly stocks and sources are in Table 1. Unless otherwise indicated, flies were maintained at 21–23°C. Embryos were collected for 1–3 hours and larvae were heat shocked 72 hours after egg laying (AEL) for 15 minutes at 37°C (Fig. 1–Fig. 3, Fig. 6C–G", Fig. 7, Fig. 8), or collected for 24 hours and heat shocked 48 to 72 hours AEL for 15 minutes (Fig. 4, Fig. 5, Fig. 6A–B, Supplementary Fig. 2–Supplementary Fig. 5). Wing discs in Fig. 1–Fig. 5, Fig. 6A–B, Fig. 7E–F were dissected at either the wandering 3rd instar stage (~96–120 hours after clone induction when maintained at 21–23°C) or at the indicated times after clone induction. For Fig. 6C–G" (*shotgun* hypomorph experiments), Fig. 7A–D, G (*UAS-sqh^{wt}* and *UAS-sqh^{EE}* experiments), and Fig. 8C–D (*UAS-Rho1^{dsRNA}* experiment), larvae were heat shocked at 72 hours AEL and dissected at 72 hours after clone induction. For Fig. 8A–B (*UAS-Rho1^{N19}* experiments), larvae were heat shocked at 72 hours AEL, maintained at 18°C after clone induction (to minimize *UAS-Rho1^{N19}* expression level), and dissected 4 days after clone induction.

Immunolocalization and microscopy

Antibodies and probes are in Table 1. Wing discs were fixed in 4% paraformaldehyde in PBS for 20 minutes. For pupal wings, pupal cases were cut open, and entire pupae were fixed in 4% formaldehyde with 0.2% Tween®20 for 30 minutes prior to wing dissection. Discs were blocked and stained in PBS with 1% goat serum and 0.1% Triton X-100. Imaging was performed on a spinning disk confocal microscope (Solamere Technology Group) with either a Hamamatsu OrcaAG CCD camera or a Qimaging Qicam-IR. Fig. 2A–A" were imaged using an Olympus Fluoview FV500 laser scanning system. Fig. 6B, B1–B3 were imaged using a Zeiss LSM 510 Meta. Images were prepared using ImageJ 1.40g and Adobe Photoshop.

Quantification and Statistics

Pixel intensity plots, measurements, Z-stack projections and optical cross-sections were prepared using ImageJ 1.40g. DE-cadherin pixel intensities were measured at tri-cellular junctions from projected images. Average apical surface areas were calculated by measuring the area in each region of interest and dividing by the number of cells in that region. Cell area ratios are ratios of the average areas in clone cells versus the average areas in neighboring non-clone cells. Nucleus size ratios were inferred by measuring the area of each nucleus in a clone and dividing by the average area of wild-type cell nuclei in either cells surrounding the clone or in wild type cells in the same location in a different disc. The optical slice in the z-axis displaying the largest cross-sectional area for each nucleus was chosen for measurement. For the statistical analysis in Fig. 8G, nucleus area ratios were binned such that if the ratio $\leq 1.50 \times$ average wild type area, then size = 1x, and similarly, if $1.50 <$ ratio ≤ 2.50, size = 2x, if $2.50 <$ ratio ≤ 3.50, size = 3x, etc. Statistics were performed

using EXCEL and SPSS. The log-normal distributions in Fig. 8E were log-transformed for statistical calculations and transformed back for data display.

Results

Loss of *APC1* and *APC2* results in cell segregation and apical constriction

To determine the consequences to epithelia of complete loss of APC, we induced clones of $APC2^{g10} APC1^{Q8}$ [*APC* null (Ahmed et al., 1998; McCartney et al., 2006 and Supplementary Fig. 1B)] cells, distinguished by their lack of GFP, in wing imaginal discs. All changes in morphology were completely suppressed by coexpressing one copy of a wild-type *APC2* transgene (McCartney et al., 2006) in *APC* null clones (Supplementary Fig. 2, and data not shown).

Up to 30 hours after clone induction (at 21–23°C), *APC* null clones have wild-type morphology, exhibiting irregular borders and a topography indistinguishable from surrounding wild-type cells (Fig. 1A, A'). By 40–42 hours after clone induction, 4% of clones have smooth borders (n=304 clones, 15 discs; Fig. 1B, arrows), suggesting that mutant cells segregate from their wild-type neighbors. Some cells in these clones appear apically constricted (inset in Fig. 1B, arrow), and some clones with apically constricted cells are beginning to invaginate (Fig. 1C, arrow). By 72 hours after clone induction, most *APC* null clones (86%; n=90 clones, 12 discs) have smooth borders and are round. At this point, clones in the presumptive blade (the wing pouch), notum, and ventral pleura are apically constricted and invaginated, and some are protruding basally (Fig. 1D–H). Control clones throughout larval development have irregular borders and a topography indistinguishable from the surrounding epithelium (Fig. 2A–A", and data not shown).

By the late third instar (96–120 hours after clone induction; n=112 clones, 12 discs), *APC* null clones in the ventral pleura and ventral hinge have invaginated and protrude basally (Fig. 2C–C", double asterisks, and data not shown). In contrast, nearly all dorsal hinge clones evaginate (protrude apically; Fig. 2B–B", single asterisks), although a few invaginate (Fig. 2B–B", double asterisks). While nearly all *APC* clones in the wing pouch and areas of the notum distal to the hinge have smooth borders and apically constrict, they typically exhibit only mild invagination by the late 3rd instar (Fig. 2D–D" and data not shown). Surprisingly, only 6 hr after puparium formation some clones within the blade have significantly invaginated and are trapped within the developing wing (Fig. 2G, H, arrows), while retaining their connections to the surrounding epithelium (Fig. 2H).

Is overproliferation responsible for the changes observed in *APC* mutant tissue?

Loss of *APC* in the disc activates Wnt signaling (Ahmed et al., 2002; Akong et al., 2002), and Wnt signaling is mitogenic in certain contexts (Giraldez and Cohen, 2003). Consistent with this, *APC* null clones that significantly invaginate/evaginate appeared to contain more cells than their wild-type twin spots (marked by two copies of GFP). We calculated the mutant clone:twin spot ratio, and compared that to the control clone:twin spot ratio from the same regions of the disc. *APC* null cells from disc regions that significantly invaginate/evaginate have approximately 2–2.5 times more cells than their twin spots (p < 0.01; Table

2). We detected little or no overproliferation in disc regions that do not significantly invaginate/evaginate (Table 2). This suggests that overproliferation could play a role in the change in morphology of *APC* null tissue.

We next asked whether overproliferation is required for apical constriction. We calculated the mutant clone:twin spot ratio in *APC* null clones exhibiting apical constriction, but mild to no invagination, between 44 and 96 hours after clone induction. If overproliferation and apical constriction are causally linked, all apically constricted clones would have a mutant clone:twin spot ratio significantly greater than 1. 72% of apically constricting clones (n=18 clones, 12 discs) exhibited a mutant clone:twin spot ratio of 1.1 or less, indicating that the apical constriction does not result from overproliferation. However, overproliferation may contribute to the extreme protrusion of many *APC* null clones in the late 3rd instar.

Canonical Wnt signaling is necessary and sufficient for the morphological changes of *APC* mutant tissue

Wing clones defective for *APC* activate canonical Wnt signaling, resulting in a fate transformation (Ahmed et al., 2002; Akong et al., 2002). However, APC proteins can also directly affect actin and microtubules (reviewed in McCartney and Nathke, 2008). We asked whether activation of the Wnt pathway independent of APC is sufficient to induce the morphological changes characteristic of *APC* null tissue. We either expressed a stabilized form of Armadillo [Arm^{S10}, (Pai et al., 1997)], or removed the negative regulator Axin, in a wild-type background. Strikingly, both recapitulate the *APC* null phenotype (Fig. 3A–D', and data not shown).

We also assessed whether activation of the Wnt pathway is necessary for triggering the *APC* null phenotype by disrupting activation of Wnt target genes with a dominant negative form of TCF (TCF ^{N}) (van de Wetering et al., 1997), a transcriptional co-activator with Armadillo. Expression of TCF ^{N} in *APC* null tissue in the posterior wing compartment suppressed the morphological changes (Fig. 3E, E', E2). Not only did TCF ^{N} prevent the apical constriction in *APC* null cells, but resulted in apical expansion (Fig. 3E2, F). This was also true for wild-type cells expressing TCF ^{N} (Fig. 3F). This suggests that the wing epithelium exhibits a basal level of apical constriction dependent on canonical Wnt signaling. This is consistent with an earlier model suggesting that the proximal-distal gradient of apical constriction in the wing imaginal disc pouch is regulated by a corresponding gradient of Wingless (Drosophila Wnt-1) (Jaiswal et al., 2006). Together, these data demonstrate that the morphological changes in *APC* null tissue depend primarily on transcriptional activation downstream of canonical Wnt signaling, rather than disruption of APC's cytoskeletal functions.

Separating cell fate and cell shape

Canonical Wnt signaling is best known for its role in establishing cell fate during development (reviewed in van Amerongen and Nusse, 2009). Consequently, we asked whether the morphological changes we observed in *APC* null clones were a primary effect of Wnt signaling, or were a secondary consequence of a change in fate of the *APC* mutant cells. *APC* mutant clones in the wing blade are known to undergo a cell fate transformation

to wing margin fate resulting from the activation of canonical Wnt signaling (Ahmed et al., 2002; Akong et al., 2002). We reasoned that if the change in cell fate and the change in cell shape were causally linked, *APC* mutant cells that did not undergo a change in their final fate would not exhibit cell shape changes. To ask if fate change could be separated from shape changes, we compared clone fate and shape of *APC* mutant cells expressing different alleles of *APC2* in combination with *APC1^{Q8}*. Based on previous work in the embryo (McCartney et al., 2006), we predicted that weaker *APC2 APC1* combinations, such as *APC2^S APC1^{Q8}* would result in weaker activation of Wnt signaling. We found that *APC* null cells ectopically activate canonical Wnt target genes including *vestigial*, *senseless*, and *distal-less* (Jafar-Nejad et al., 2006; Neumann and Cohen, 1997; Parker et al., 2002; Zecca et al., 1996) (Fig. 4A–B and Supplementary Fig. 3A–D). In contrast, *APC2^S APC1^{Q8}* mutant cells exhibited weaker activation of target genes, occasionally activating *senseless* (Fig. 4C–D, arrows), but not *vestigial* and *distal-less* (data not shown).

Consistent with a strong activation of Wnt signaling, *APC* null tissue, or that expressing strong hypomorphic *APC2* alleles such as *APC2^{d40} APC1^{Q8}* (Ahmed et al., 2002; Akong et al., 2002), in the adult wing exhibits the predicted fate transformation (Fig. 4E, F). Interestingly, while most cells in *APC* null clones undergo this fate change, some do not (Fig. 4F, arrowheads). Other strong allelic combinations exhibit cell shape and cell fate transformation similar to *APC* null (Supplementary Fig. 4E, E', F, F', and data not shown). Consistent with the weaker activation of canonical Wnt targets in the *APC2^S APC1^{Q8}* cells, *APC2^S APC1^{Q8}* clones in the blade, or those expressing another weak allele of *APC2, APC2^{N175K} APC1^{Q8}*, do not transform to margin (Fig. 4G, and data not shown). *APC2^S APC1^{Q8} and APC2^{N175K} APC1^{Q8}* cells retain blade fate.

If the morphological changes in *APC* null cells are the result of their fate transformation from blade to margin, we predicted that *APC2^S APC1^{Q8}* and *APC2^{N175K} APC1^{Q8}* cells would not undergo shape change. However, these mutants did exhibit morphological changes, including apical constriction, in some clones (Fig. 4H, H', Supplementary Fig. 4D, D'). The reduced frequency of *APC2^S APC1^{Q8}* clones with morphological changes compared to *APC2^{g10} APC1^{Q8}* (35% n= 339 clones, 30 discs compared to 84% n= 112 clones, 12 discs, respectively) suggests that the amount of Wnt signaling in *APC2^S APC1^{Q8}* cells is at a threshold for morphological changes. Similarly, other weak alleles of *APC2*, including *APC2^{b5}* and *APC2^{e90}* (McCartney et al., 2006), exhibit weak morphological changes or no morphological changes (Supplementary Fig. 4A–B', G). Together, these data suggest that the morphological changes are not a result of the cell fate transformation from blade to margin. Transcriptional activation downstream of the canonical Wnt pathway appears to exert a more direct effect on cell shape.

Apical constriction of *APC* null cells is correlated with DE-cadherin upregulation

How does activation of the canonical Wnt pathway induce smooth clone borders, apical constriction and invagination? Smooth borders suggest adhesive differences between cells of different genotypes. Changes in cadherin-based or Echinoid-based adhesion can cause smooth borders and may contribute to apical constriction in wing discs (Dahmann and Basler, 2000; Jaiswal et al., 2006; Wei et al., 2005). Apical constriction itself may also

contribute to smooth borders (Wei et al., 2005). One study reported a correlation between the proximal-distal gradient of Wingless, *DE-cadherin* (*DE-cad*) transcriptional upregulation, DE-cad protein accumulation, and apical constriction in the wing pouch (Jaiswal et al., 2006). They further reported that DE-cad overexpression clones apically constricted, suggesting a causal relationship between Wnt pathway activation, elevated DE-cad, and apical constriction (Jaiswal et al., 2006). Others have also reported that *DE-cad* is a transcriptional target of Wnt signaling (Wodarz et al., 2006). Together, this suggested that at least some of the *APC* null morphological changes could be due to Wnt-mediated upregulation of *DE-cad*. Surprisingly, while *DE-cad-lacZ* reporter activity (as detected by immunolocalization of β-galactosidase) is elevated in some *APC* mutant cells (Fig. 5A, B; 20/25 of clones exhibit elevation in at least some cells), there appears to be an inverse relationship between apical constriction and elevation of the β-galactosidase; cells that are apically constricted do not tend to express the β-galactosidase (Fig. 5A, A1, B, B1, arrows) while some cells that are not apically constricted exhibit robust elevation of β-galactosidase (Fig. 5A, A1, A2, arrowheads).

Despite the lack of correlation between activation of the *DE-cad-lacZ* reporter and apical constriction, we predicted that if there is a causal relationship between elevated DE-cad protein and apical constriction, all apically constricted cells should display elevated DE-cad. Qualitatively we found that while some apically constricted cells had a significant apparent increase in DE-cad (Fig. 1E–F'), others did not (Fig. 1G–H'). However, when we quantitatively assessed DE-cad protein levels and compared that to the degree of constriction in *APC* null cells we found a strong correlation (Fig. 5C). These data suggest that, although apical constriction may be correlated with an increase in concentration of DE-cad in at the adherens junctions, this localized increase may not require transcriptional upregulation or an increase in overall cellular levels of DE-cad protein. Rather, the apparent localized increase could be due to passive concentration of DE-cad resulting from apical constriction, and not the result of an active increase in DE-cad levels. This may be consistent with the absence of *DE-cad-lacZ* activation in apically constricting cells. Regardless of the mechanism, the apparent elevation of DE-cad protein at the adherens junctions could contribute to the smooth borders, apical constriction, and invagination of *APC* null cells.

DE-cad elevation is not sufficient to recapitulate the *APC* null morphology

To test whether elevated DE-cad is sufficient to induce the smooth borders, apical constriction, and invagination characteristic of *APC* null tissue, we overexpressed DE-cad in clones wild type for *APC*. We did not predict that overexpression of DE-cad alone would produce the extreme protrusion exhibited by some *APC* null clones because overproliferation may contribute to the protrusion of *APC* null clones (Table 2). To vary the amount of overexpression, we maintained larvae at either 18°C after clone induction (expression comparable to or lower than in *APC* null cells; compare Fig. 1E, G to Supplementary Fig. 5A–A1') or 21 – 23°C after clone induction (expression comparable to or higher than in *APC* null cells; compare Fig. 1E, G to Fig. 6A, B). With lower elevation of DE-cad, 99% of clones were morphologically normal, with no apical constriction, or invagination/evagination (n=89 clones, 23 discs, Supplementary Fig. 5A–A1'). Clone borders were smoother than in wild-type clones, but clone cells did sometimes interdigitate

with non-clone cells (Supplementary Fig. 5A, A1, arrow). With higher elevation of DE-cad, 94% of the clones were morphologically normal, with no invagination/evagination (Fig. 6A, B; n=139 clones, 44 discs). Approximately half of these otherwise morphologically normal clones had smooth borders (Fig. 6A; uneven border, Fig. 6B, B1; smooth border), but none were round like *APC* null clones. Most clones (>99%) did not apically constrict (Fig. 6B2, B3); only one clone exhibited mildly constricted cells (Supplementary Fig. 5B–B2). 6% of clones with highly elevated DE-cad protruded or otherwise misfolded (Supplementary Fig. 5C–E"). Of these 6%, none displayed coordinated apical constriction, and only 3 clones (2% of total) were round like *APC* null clones (Supplementary Fig. 5E–E''). Thus, despite the fact that DE-cad appears elevated in *APC* null clones, increased DE-cad expression, at levels comparable to or higher than what we observe in *APC* null cells, is not sufficient to recapitulate the *APC* null phenotype.

DE-cad elevation is not necessary for the development of *APC* null morphology

While elevation of DE-cad is not sufficient, it may be necessary for the *APC* null phenotype. To test this, we induced clones that were *APC* null and homozygous for a *DE-cad* hypomorph, *shotgun^{p34-1}* (*shg $^{p34-1}$*). *shg $^{p34-1}$* clones in a wild-type background have smoother borders than wild-type clones (compare Fig. 6C with Fig. 2A–A'). Otherwise, *shg $^{p34-1}$* cells appeared wild-type, suggesting that they retain intact adherens junctions, consistent with previous results (Le Borgne et al., 2002). If elevation of DE-cad is necessary for apical constriction in *APC* null cells, *APC* null cells expressing less DE-cad than wild-type will not constrict. *shg^{p34-1}*; *APC2^{g10} APC1^{Q8}* cells exhibit levels of DE-cad lower than the surrounding *shg^{p34-1}/+; APC2^{g10} APC1^{Q8}/+* cells. However, these clones exhibit smooth borders, apically constrict, and invaginate (in 19 discs, 20/20 clones have smooth borders and apically constrict, and 19/20 clones invaginate; Fig. 6D–F"), similar to *shg$^+$*; *APC2^{g10} APC1^{Q8}* cells (Fig. 6G–G"). Contradictory to the earlier model of the relationship between Wnt signaling, DE-cad, and apical constriction (Jaiswal et al., 2006), our data taken together indicate that DE-cad elevation is neither necessary nor sufficient for the apical constriction and invagination of *APC* mutant clones.

Myosin II activity is necessary for apical constriction of *APC* null cells

Apical constriction of *APC* null cells (e.g. Fig. 1E) resembles the cell shape changes triggered by actomyosin contraction, a well-described mechanism contributing to apical constriction (reviewed in Pilot and Lecuit, 2005; Young et al., 1991). In *Drosophila*, activation of non-muscle Myosin II (MyoII) is induced by phosphorylation of the myosin regulatory light chain Spaghetti squash (Sqh) (reviewed in Matsumura, 2005; Tan et al., 1992). Sqh has two activating phosphorylation sites at Ser-21 and Thr-20 (Jordan and Karess, 1997; Winter et al., 2001).

Expression of the constitutively active Sqh^{EE} (Jordan and Karess, 1997; Kirchner et al., 2007), is sufficient for apical constriction and invagination in the wing imaginal epithelium (Fig. 7C–C", D), but the clones are not round like *APC* null clones (Fig. 7C–C",D). Expression of Sqh^{wt} had no effect on cell morphology (Fig. 7A, B). Consistent with a role for active MyoII in *APC* null apical constriction, the doubly phosphorylated form of Sqh, but not total Sqh or singly phosphorylated Sqh, was enriched in apically constricting *APC*

null cells (Zimmerman and McCartney, unpublished observations). Expression of a mutant form of Sqh in which both Ser-21 and Thr-20 have been replaced by alanines (Sqh^{AA}) (Jordan and Karess, 1997; Kirchner et al., 2007) in *APC* null cells suppressed apical constriction (Fig. 7F, G, H). In wild type cells, Sqh^{AA} expression results in weak apical expansion (Fig. 7E, H). These data indicate that MyoII activity is necessary for the apical constriction of *APC* null cells.

Rho1 signaling is required for apical constriction of *APC* null cells

Activation of MyoII is often downstream of Rho pathway activity. If apical constriction in *APC* null cells depends on Rho1 signaling, disrupting Rho1 will suppress apical constriction. To test this, we expressed a dominant negative form of Rho1, *UAS-Rho1^{N19}*, in wild type cells and in *APC* null cells. This tool has been widely used to disrupt Rho1 signaling (Hozumi et al., 2006; Simoes et al., 2006; Strutt et al., 1997). In wild type cells expressing Rho1^{N19}, we observed apically expanded, abnormally large cells (Fig. 8A, E) that were likely the result of cytokinesis failure; a significant portion of the nuclei were abnormal (Fig. 8A, A'), ranging up to 5x the size of the surrounding wild type nuclei (Fig. 8A', F, n=188 nuclei in 12 clones). The apical expansion of *UAS-Rho1^{N19}* cells may be the result of cytokinesis defects coupled with an inability to generate the basal level of apical constriction.

APC null cells expressing *UAS-Rho1^{N19}* were not apically constricted but moderately expanded compared to surrounding wild-type cells (Fig. 8B, E). This is similar to *APC* null cells expressing TCF ^{N} (Fig. 3E', F), Sqh^{AA} (Fig. 7F, H), or a double-stranded RNA against *Rho1* (Fig. 8C, C', E). Although expanded, most of the *UAS-Rho1^{N19}/+; APC2^{g10} APC1^{Q8}* and *UAS-Rho1^{dsRNA}/+; APC2^{g10} APC1^{Q8}* cells appeared to have normal sized nuclei (Fig. 8B' compared with inset, Fig. 8C'' compared with 7D) consistent with normal cytokinesis. Of those nuclei that were abnormal, there were fewer severely enlarged nuclei compared to *UAS-Rho1^{N19}/+; +/+* cells (Fig. 8F, G). Thus, we conclude that the expansion we observe in *APC* null cells expressing either Rho1^{N19} or the *Rho1^{dsRNA}* is not due primarily to defects in cytokinesis. These data suggest that Rho1 is required for apical constriction in *APC* null cells.

Interestingly, the *UAS-Rho1^{N19}/+; APC2^{g10} APC1^{Q8}* phenotype is less severe than the *UAS-Rho1^{N19}/+; +/+* phenotype; apical expansion is suppressed (Fig. 8E), and the severity of the nuclear defects is reduced (Fig. 8F, G). Because *APC* null cells are more constricted than wild type cells, and Rho1^{N19} expressing cells are more expanded than wild type, the apparent mutual suppression could reflect a synergistic effect. However, suppression of the Rho1^{N19} nuclear defects in *APC* null cells suggests a specific interaction between the canonical Wnt pathway and the Rho1 pathway.

Discussion

Tissue morphogenesis involves the coordinated activity of signaling pathways, which instruct or permit shape change, and the downstream cytoskeletal players that affect cell and tissue shape changes. The molecular basis for this coordination is poorly understood. We have shown that loss of *APC* and activation of canonical Wnt signaling leads to striking

morphological changes in the wing epithelium; most *APC* null clones develop smooth borders and segregate, and apically constrict and invaginate, resulting in basal extrusion. Wnt-dependent segregation of *APC* null tissue also occurs in the *Drosophila* larval optic lobe epithelia, although the molecular requirements for that phenotype were not described (Hayden et al., 2007).

Non-canonical Wnt planar cell polarity (PCP) signaling is essential for convergent extension (Heisenberg et al., 2000; Wallingford et al., 2000), and promotes primary invagination in the sea urchin archenteron (Croce et al., 2006). Wnt signaling is implicated in apical constriction of endoderm during *C. elegans* gastrulation (Lee et al., 2006), but whether the Wnt, MOM-2, acts through the canonical or non-canonical pathway is not known. Canonical Wnt signaling is connected to other morphogenetic movements, including *Drosophila* dorsal closure (McEwen et al., 2000; Morel and Martinez Arias, 2004), zebrafish neurulation (Nyholm et al., 2009), and epithelial cell elongation in the wing disc (Widmann and Dahmann, 2009), though whether this results from effects on cell fate is unclear. In contrast, we can genetically decouple fate and morphogenesis, observing morphological changes in the absence of fate changes from blade to margin (Fig. 4G, H, H', Supplementary Fig. 4D, D'). Thus, our data provide a first example of how transcriptional activation downstream of canonical Wnt signaling directly affects cell morphology.

Wnt-induced morphology changes do not require elevated DE-cad

The proximal-distal gradient of Wingless (Wg; *Drosophila* Wnt-1) extending from the presumptive wing margin in the imaginal disc correlates with a proximal-distal gradient of cell shape, and it has been suggested that this Wg gradient causes apical constriction of the cells at or near the wing margin through Wg-dependent transcriptional upregulation of DE-cad (Jaiswal et al., 2006). Thus, we predicted that the morphological changes in *APC* mutant tissue resulted from DE-cad-based adhesive differences between the *APC* mutant and wild type cells due to an elevation of DE-cad protein at the adherens junctions of *APC* mutant cells. Although DE-cad is transcriptionally upregulated in some *APC* mutant clones, and the protein appears to accumulate to higher levels than wild type (Fig. 5C and data not shown), elevated DE-cad is not necessary for the Wnt-induced morphological changes (Fig. 6D–F"). Finally, while we observed smoother clone borders in tissue ectopically overexpressing DE-cad, none exhibited the apical constriction and invagination characteristic of *APC* mutant tissue (Fig. 6A–B3, Supplementary Fig. 5). This is in contrast to a previous report that DE-cad overexpression clones apically constrict (Jaiswal et al., 2006, p. 927). Thus, while DE-cad appears elevated in *APC* mutant tissue, this elevation does not appear to contribute significantly to the apical constriction and invagination we observe. Because it is likely that functional adherens junctions are a basic requirement for cells to apically constrict (Dawes-Hoang et al., 2005; Martin et al., 2009), the baseline level, but not an elevated level, of DE-cad based adhesion is likely required for apical constriction in this system as well.

Canonical Wnt signaling requires Rho1 and Myosin II to induce apical constriction

One of the most well-described mechanisms driving apical constriction is actomyosin based contractility (reviewed in Pilot and Lecuit, 2005). Our data suggest that actomyosin-based contraction plays an important role in apical constriction in *APC* mutant epithelia (Fig. 7).

MRLC is the target of many known kinases (reviewed in Matsumura, 2005). Downstream of Rho, both Rho kinase (Rok) and citron kinase (Sticky in *Drosophila*) can phosphorylate MRLC at the 1° and 2° sites (reviewed in Jordan and Karess, 1997; Matsumura, 2005). In apical constriction, the Rho1-Rok–MyoII cassette operates in the follicular epithelium during oogenesis (Wang and Riechmann, 2007), and in the morphogenetic furrow in the eye imaginal disc (Corrigall et al., 2007; Escudero et al., 2007).

Functionally, Rho1 is required for apical constriction in *APC* mutant cells, and the dominant negative Rho1 phenotype is suppressed in *APC* mutant cells. One interpretation of these data is that Wnt signaling and Rho signaling are in a linear pathway where increased Wnt signaling promotes increased Rho1 activity (Supplementary Fig. 6A). In this model, Wnt signaling increases the pool of Rho1-GTP, thereby mitigating all of the effects of Rho1 disruption. An alternative interpretation is the parallel model (Supplementary Fig. 6B): Wnt signaling and Rho1 signaling independently promote MyoII activation and apical constriction. Suppression by loss of *APC* of both the apical expansion and the nuclear defects in $Rho1^{N19}$ cells can be explained by a Wnt-dependent increase in active MyoII. However, because Rho1 also promotes cytokinesis via formins (reviewed in Piekny et al., 2005), increasing active MyoII alone may not be sufficient to suppress Rho1 defects in cytokinesis. While the suppression of the *APC* mutant phenotype by disruption of Rho1 is consistent with either a parallel or a linear model, the suppression of the Rho1 cytokinesis defects by loss of *APC* provides some additional evidence in support of the linear model. Further investigation will resolve this issue. Regardless of the precise role of Rho1 in canonical Wnt-dependent apical constriction, the pathway ultimately requires activated MyoII. Interestingly, disruption of Wnt signaling in wild type wing epithelial cells results in apical expansion (Fig. 3F), consistent with a role for Wnt signaling in maintaining a basal level of MyoII-dependent apical constriction.

Our findings connecting canonical Wnt signaling to MyoII activity are consistent with very recent work suggesting a link between canonical Wnt transcriptional activation and MyoII in the development of the dorsolateral hinge points during zebrafish neurulation (Nyholm et al., 2009). While the Wnt-PCP pathway has a well-known connection to Rho and MyoII (reviewed in Simons and Mlodzik, 2008; Winter et al., 2001), connections between the canonical Wnt pathway and the Rho-MyoII cassette have not been previously identified. Interestingly, two transcription factors that regulate apical constriction upstream of Rho1, Twist and Snail (Ip et al., 1994; Leptin, 1991; Leptin and Grunewald, 1990; Martin et al., 2009; Seher et al., 2007), are also transcriptional targets of canonical Wnt signaling in vertebrates and *Drosophila* (Bate and Rushton, 1993; Howe et al., 2003; ten Berge et al., 2008). *twist* and *snail* are thus good candidates for a role in Wnt-dependent apical constriction.

The role of apical constriction and invagination in the development of intestinal polyps

Mutations in human *APC* cause an inherited form of colorectal cancer (CRC), and are found in approximately 85% of sporadic CRCs (reviewed in Pinto and Clevers, 2005). The mammalian intestinal epithelium is organized into distinct compartments (Supplementary Fig. 6C); the proliferative compartment (crypt) contains the stem cells/progenitor cells, and

the differentiated compartment (the villus [small intestine], and the flat surface epithelium [large intestine]), contains primarily absorptive and endocrine cells (reviewed in Sancho et al., 2004). Canonical Wnt signaling controls cell fate and compartmentalization along the crypt-villus axis, and maintains cells in the proliferative state (reviewed in Pinto and Clevers, 2005). Disruption of *APC* in the intestine of adult mice results in the accumulation of crypt-like cells that fail to differentiate (Sansom et al., 2004), leading to the formation of benign polyps or adenomas (reviewed in Pinto and Clevers, 2005). Interestingly, *APC* mutant tissue "outpockets" and "buds" in both the mouse intestine, and the mouse and human colon (Oshima et al., 1997; Preston et al., 2003). This results in basal extrusion, and the developing polyp becomes trapped between normal epithelium and basement membrane (Supplementary Fig. 6C–E).

Some of these changes in tissue organization are the result of Eph signaling downstream of canonical Wnt pathway activation in *APC* mutant cells (Cortina et al., 2007). Colorectal cancer (CRC) cells in culture "contract" and pack into "tight clusters" in response to EphB signaling. While the clustering is dependent on E-cadherin, the contraction requires a distinct mechanism. *APC* mutant epithelia in *Drosophila* have smooth borders with the surrounding wild-type epithelia (Fig. 1E), analogous to the clustering of CRC cells. While elevated DE-cad does not contribute to apical constriction and invagination in *APC* null cells (Fig. 6), differences in DE-cad adhesion could be a factor in segregation. Our data suggest that the contraction of CRC cells (Cortina et al., 2007) may be an acto-myosin based cell shape change downstream of Rho signaling.

Given the similarities in response of these distinct epithelia to the activation of canonical Wnt signaling, it is tempting to speculate that some of the same cellular machinery is deployed downstream of Wnt signaling in both the imaginal disc and the mammalian intestinal epithelium. We predict that the imaginal disc will be a powerful model to address the role of Wnt signaling in cell and tissue morphogenesis, both in normal development and in tumorigenesis.

Supplementary Material

Refer to Web version on PubMed Central for supplementary material.

Acknowledgments

References

Ahmed Y, Hayashi S, Levine A, Wieschaus E. Regulation of armadillo by a Drosophila APC inhibits neuronal apoptosis during retinal development. Cell. 1998; 93:1171–1182. [PubMed: 9657150]

Ahmed Y, Nouri A, Wieschaus E. Drosophila Apc1 and Apc2 regulate Wingless transduction throughout development. Development. 2002; 129:1751–1762. [PubMed: 11923210]

Akong K, Grevengoed EE, Price MH, McCartney BM, Hayden MA, DeNofrio JC, Peifer M. Drosophila APC2 and APC1 play overlapping roles in wingless signaling in the embryo and imaginal discs. Dev Biol. 2002; 250:91–100. [PubMed: 12297098]

Bate, M.; Martinez Arias, A. The Development of Drosophila melanogaster. Vol. Vol. 2. Plainview, NY: Cold Spring Harbor Laboratory Press; 1993. p. 1558

Bate M, Rushton E. Myogenesis and muscle patterning in Drosophila. C R Acad Sci III. 1993; 316:1047–1061. [PubMed: 8076205]

Cadigan KM, Nusse R. Wnt signaling: a common theme in animal development. Genes Dev. 1997; 11:3286–3305. [PubMed: 9407023]

Casares F, Mann RS. A dual role for homothorax in inhibiting wing blade development and specifying proximal wing identities in Drosophila. Development. 2000; 127:1499–1508. [PubMed: 10704395]

Corrigall D, Walther RF, Rodriguez L, Fichelson P, Pichaud F. Hedgehog signaling is a principal inducer of Myosin-II-driven cell ingression in Drosophila epithelia. Dev Cell. 2007; 13:730–742. [PubMed: 17981140]

Cortina C, Palomo-Ponce S, Iglesias M, Fernandez-Masip JL, Vivancos A, Whissell G, Huma M, Peiro N, Gallego L, Jonkheer S, Davy A, Lloreta J, Sancho E, Batlle E. EphB-ephrin-B interactions suppress colorectal cancer progression by compartmentalizing tumor cells. Nat Genet. 2007; 39:1376–1383. [PubMed: 17906625]

Couso JP, Bishop SA, Martinez Arias A. The wingless signalling pathway and the patterning of the wing margin in Drosophila. Development. 1994; 120:621–636. [PubMed: 8162860]

Croce J, Duloquin L, Lhomond G, McClay DR, Gache C. Frizzled5/8 is required in secondary mesenchyme cells to initiate archenteron invagination during sea urchin development. Development. 2006; 133:547–557. [PubMed: 16396908]

Dahmann C, Basler K. Opposing transcriptional outputs of Hedgehog signaling and engrailed control compartmental cell sorting at the Drosophila A/P boundary. Cell. 2000; 100:411–422. [PubMed: 10693758]

Dawes-Hoang RE, Parmar KM, Christiansen AE, Phelps CB, Brand AH, Wieschaus EF. folded gastrulation, cell shape change and the control of myosin localization. Development. 2005; 132:4165–4178. [PubMed: 16123312]

Escudero LM, Bischoff M, Freeman M. Myosin II regulates complex cellular arrangement and epithelial architecture in Drosophila. Dev Cell. 2007; 13:717–729. [PubMed: 17981139]

Gibson MC, Schubiger G. Drosophila peripodial cells, more than meets the eye? Bioessays. 2001; 23:691–697. [PubMed: 11494317]

Giraldez AJ, Cohen SM. Wingless and Notch signaling provide cell survival cues and control cell proliferation during wing development. Development. 2003; 130:6533–6543. [PubMed: 14660542]

Green RA, Kaplan KB. Chromosome instability in colorectal tumor cells is associated with defects in microtubule plus-end attachments caused by a dominant mutation in APC. J Cell Biol. 2003; 163:949–961. [PubMed: 14662741]

Hayden MA, Akong K, Peifer M. Novel roles for APC family members and Wingless/Wnt signaling during Drosophila brain development. Dev Biol. 2007; 305:358–376. [PubMed: 17367777]

Heisenberg CP, Tada M, Rauch GJ, Saude L, Concha ML, Geisler R, Stemple DL, Smith JC, Wilson SW. Silberblick/Wnt11 mediates convergent extension movements during zebrafish gastrulation. Nature. 2000; 405:76–81. [PubMed: 10811221]

Howe LR, Watanabe O, Leonard J, Brown AM. Twist is up-regulated in response to Wnt1 and inhibits mouse mammary cell differentiation. Cancer Res. 2003; 63:1906–1913. [PubMed: 12702582]

Hozumi S, Maeda R, Taniguchi K, Kanai M, Shirakabe S, Sasamura T, Speder P, Noselli S, Aigaki T, Murakami R, Matsuno K. An unconventional myosin in Drosophila reverses the default handedness in visceral organs. Nature. 2006; 440:798–802. [PubMed: 16598258]

Ip YT, Maggert K, Levine M. Uncoupling gastrulation and mesoderm differentiation in the Drosophila embryo. Embo J. 1994; 13:5826–5834. [PubMed: 7813421]

Jafar-Nejad H, Tien AC, Acar M, Bellen HJ. Senseless and Daughterless confer neuronal identity to epithelial cells in the Drosophila wing margin. Development. 2006; 133:1683–1692. [PubMed: 16554363]

Jaiswal M, Agrawal N, Sinha P. Fat and Wingless signaling oppositely regulate epithelial cell-cell adhesion and distal wing development in Drosophila. Development. 2006; 133:925–935. [PubMed: 16452097]

Jordan P, Karess R. Myosin light chain-activating phosphorylation sites are required for oogenesis in Drosophila. J Cell Biol. 1997; 139:1805–1819. [PubMed: 9412474]

Kawasaki Y, Senda T, Ishidate T, Koyama R, Morishita T, Iwayama Y, Higuchi O, Akiyama T. Asef, a link between the tumor suppressor APC and G-protein signaling. Science. 2000; 289:1194–1197. [PubMed: 10947987]

Kirchner J, Gross S, Bennett D, Alphey L. The nonmuscle myosin phosphatase PP1beta (flapwing) negatively regulates Jun N-terminal kinase in wing imaginal discs of Drosophila. Genetics. 2007; 175:1741–1749. [PubMed: 17277363]

Kita K, Wittmann T, Nathke IS, Waterman-Storer CM. Adenomatous polyposis coli on microtubule plus ends in cell extensions can promote microtubule net growth with or without EB1. Mol Biol Cell. 2006; 17:2331–2345. [PubMed: 16525027]

Kroboth K, Newton IP, Kita K, Dikovskaya D, Zumbrunn J, Waterman-Storer CM, Nathke IS. Lack of adenomatous polyposis coli protein correlates with a decrease in cell migration and overall changes in microtubule stability. Mol Biol Cell. 2007; 18:910–918. [PubMed: 17192415]

Le Borgne R, Bellaiche Y, Schweisguth F. Drosophila E-cadherin regulates the orientation of asymmetric cell division in the sensory organ lineage. Curr Biol. 2002; 12:95–104. [PubMed: 11818059]

Lee JY, Marston DJ, Walston T, Hardin J, Halberstadt A, Goldstein B. Wnt/Frizzled signaling controls C. elegans gastrulation by activating actomyosin contractility. Curr Biol. 2006; 16:1986–1997. [PubMed: 17055977]

Leptin M. twist and snail as positive and negative regulators during Drosophila mesoderm development. Genes Dev. 1991; 5:1568–1576. [PubMed: 1884999]

Leptin M, Grunewald B. Cell shape changes during gastrulation in Drosophila. Development. 1990; 110:73–84. [PubMed: 2081472]

Martin AC, Kaschube M, Wieschaus EF. Pulsed contractions of an actin-myosin network drive apical constriction. Nature. 2009; 457:495–499. [PubMed: 19029882]

Matsumura F. Regulation of myosin II during cytokinesis in higher eukaryotes. Trends Cell Biol. 2005; 15:371–377. [PubMed: 15935670]

McCartney BM, Nathke IS. Cell regulation by the Apc protein Apc as master regulator of epithelia. Curr Opin Cell Biol. 2008; 20:186–193. [PubMed: 18359618]

McCartney BM, Price MH, Webb RL, Hayden MA, Holot LM, Zhou M, Bejsovec A, Peifer M. Testing hypotheses for the functions of APC family proteins using null and truncation alleles in Drosophila. Development. 2006; 133:2407–2418. [PubMed: 16720878]

McClure KD, Schubiger G. Developmental analysis and squamous morphogenesis of the peripodial epithelium in Drosophila imaginal discs. Development. 2005; 132:5033–5042. [PubMed: 16236766]

McEwen DG, Cox RT, Peifer M. The canonical Wg and JNK signaling cascades collaborate to promote both dorsal closure and ventral patterning. Development. 2000; 127:3607–3617. [PubMed: 10903184]

Morel V, Martinez Arias A. Armadillo/beta-catenin-dependent Wnt signalling is required for the polarisation of epidermal cells during dorsal closure in Drosophila. Development. 2004; 131:3273–3283. [PubMed: 15226252]

Neumann CJ, Cohen SM. Distinct mitogenic and cell fate specification functions of wingless in different regions of the wing. Development. 1996; 122:1781–1789. [PubMed: 8674417]

Neumann CJ, Cohen SM. Long-range action of Wingless organizes the dorsal-ventral axis of the Drosophila wing. Development. 1997; 124:871–880. [PubMed: 9043068]

Nyholm MK, Abdelilah-Seyfried S, Grinblat Y. A novel genetic mechanism regulates dorsolateral hinge-point formation during zebrafish cranial neurulation. J Cell Sci. 2009; 122:2137–2148. [PubMed: 19470582]

Oshima H, Oshima M, Kobayashi M, Tsutsumi M, Taketo MM. Morphological and molecular processes of polyp formation in Apc(delta716) knockout mice. Cancer Res. 1997; 57:1644–1649. [PubMed: 9135000]

Pai LM, Orsulic S, Bejsovec A, Peifer M. Negative regulation of Armadillo, a Wingless effector in Drosophila. Development. 1997; 124:2255–2266. [PubMed: 9187151]

Parker DS, Jemison J, Cadigan KM. Pygopus, a nuclear PHD-finger protein required for Wingless signaling in Drosophila. Development. 2002; 129:2565–2576. [PubMed: 12015286]

Piekny A, Werner M, Glotzer M. Cytokinesis: welcome to the Rho zone. Trends Cell Biol. 2005; 15:651–658. [PubMed: 16243528]

Pilot F, Lecuit T. Compartmentalized morphogenesis in epithelia: from cell to tissue shape. Dev Dyn. 2005; 232:685–694. [PubMed: 15712202]

Pinto D, Clevers H. Wnt control of stem cells and differentiation in the intestinal epithelium. Exp Cell Res. 2005; 306:357–363. [PubMed: 15925592]

Preston SL, Wong WM, Chan AO, Poulsom R, Jeffery R, Goodlad RA, Mandir N, Elia G, Novelli M, Bodmer WF, Tomlinson IP, Wright NA. Bottom-up histogenesis of colorectal adenomas: origin in the monocryptal adenoma and initial expansion by crypt fission. Cancer Res. 2003; 63:3819–3825. [PubMed: 12839979]

Ransom, R. A handbook of Drosophila development. Amsterdam; New York: Elsevier Biomedical Press; 1982. p. 289

Reilein A, Nelson WJ. APC is a component of an organizing template for cortical microtubule networks. Nat Cell Biol. 2005; 7:463–473. [PubMed: 15892196]

Reya T, Clevers H. Wnt signalling in stem cells and cancer. Nature. 2005; 434:843–850. [PubMed: 15829953]

Sancho E, Batlle E, Clevers H. Signaling pathways in intestinal development and cancer. Annu Rev Cell Dev Biol. 2004; 20:695–723. [PubMed: 15473857]

Sansom OJ, Reed KR, Hayes AJ, Ireland H, Brinkmann H, Newton IP, Batlle E, Simon-Assmann P, Clevers H, Nathke IS, Clarke AR, Winton DJ. Loss of Apc in vivo immediately perturbs Wnt signaling, differentiation, and migration. Genes Dev. 2004; 18:1385–1390. [PubMed: 15198980]

Seher TC, Narasimha M, Vogelsang E, Leptin M. Analysis and reconstitution of the genetic cascade controlling early mesoderm morphogenesis in the Drosophila embryo. Mech Dev. 2007; 124:167–179. [PubMed: 17267182]

Simoes S, Denholm B, Azevedo D, Sotillos S, Martin P, Skaer H, Hombria JC, Jacinto A. Compartmentalisation of Rho regulators directs cell invagination during tissue morphogenesis. Development. 2006; 133:4257–4267. [PubMed: 17021037]

Simons M, Mlodzik M. Planar cell polarity signaling: from fly development to human disease. Annu Rev Genet. 2008; 42:517–540. [PubMed: 18710302]

Struhl G, Basler K. Organizing activity of wingless protein in Drosophila. Cell. 1993; 72:527–540. [PubMed: 8440019]

Strutt DI, Weber U, Mlodzik M. The role of RhoA in tissue polarity and Frizzled signalling. Nature. 1997; 387:292–295. [PubMed: 9153394]

Tan JL, Ravid S, Spudich JA. Control of nonmuscle myosins by phosphorylation. Annu Rev Biochem. 1992; 61:721–759. [PubMed: 1497323]

ten Berge D, Koole W, Fuerer C, Fish M, Eroglu E, Nusse R. Wnt signaling mediates self-organization and axis formation in embryoid bodies. Cell Stem Cell. 2008; 3:508–518. [PubMed: 18983966]

van Amerongen R, Nusse R. Towards an integrated view of Wnt signaling in development. Development. 2009; 136:3205–3214. [PubMed: 19736321]

van de Wetering M, Cavallo R, Dooijes D, van Beest M, van Es J, Loureiro J, Ypma A, Hursh D, Jones T, Bejsovec A, Peifer M, Mortin M, Clevers H. Armadillo coactivates transcription driven by the product of the Drosophila segment polarity gene dTCF. Cell. 1997; 88:789–799. [PubMed: 9118222]

Wallingford JB, Rowning BA, Vogeli KM, Rothbacher U, Fraser SE, Harland RM. Dishevelled controls cell polarity during Xenopus gastrulation. Nature. 2000; 405:81–85. [PubMed: 10811222]

Wang Y, Riechmann V. The role of the actomyosin cytoskeleton in coordination of tissue growth during Drosophila oogenesis. Curr Biol. 2007; 17:1349–1355. [PubMed: 17656094]

Watanabe T, Wang S, Noritake J, Sato K, Fukata M, Takefuji M, Nakagawa M, Izumi N, Akiyama T, Kaibuchi K. Interaction with IQGAP1 links APC to Rac1, Cdc42, and actin filaments during cell polarization and migration. Dev Cell. 2004; 7:871–883. [PubMed: 15572129]

Webb RL, Zhou MN, McCartney BM. A novel role for an APC2-Diaphanous complex in regulating actin organization in Drosophila. Development. 2009; 136:1283–1293. [PubMed: 19279137]

Wei SY, Escudero LM, Yu F, Chang LH, Chen LY, Ho YH, Lin CM, Chou CS, Chia W, Modolell J, Hsu JC. Echinoid is a component of adherens junctions that cooperates with DE-Cadherin to mediate cell adhesion. Dev Cell. 2005; 8:493–504. [PubMed: 15809032]

Wen Y, Eng CH, Schmoranzer J, Cabrera-Poch N, Morris EJ, Chen M, Wallar BJ, Alberts AS, Gundersen GG. EB1 and APC bind to mDia to stabilize microtubules downstream of Rho and promote cell migration. Nat Cell Biol. 2004; 6:820–830. [PubMed: 15311282]

Widmann TJ, Dahmann C. Wingless signaling and the control of cell shape in Drosophila wing imaginal discs. Dev Biol. 2009; 334:161–173. [PubMed: 19627985]

Winter CG, Wang B, Ballew A, Royou A, Karess R, Axelrod JD, Luo L. Drosophila Rho-associated kinase (Drok) links Frizzled-mediated planar cell polarity signaling to the actin cytoskeleton. Cell. 2001; 105:81–91. [PubMed: 11301004]

Wodarz A, Stewart DB, Nelson WJ, Nusse R. Wingless signaling modulates cadherin-mediated cell adhesion in Drosophila imaginal disc cells. J Cell Sci. 2006; 119:2425–2434. [PubMed: 16720643]

Young PE, Pesacreta TC, Kiehart DP. Dynamic changes in the distribution of cytoplasmic myosin during Drosophila embryogenesis. Development. 1991; 111:1–14. [PubMed: 1901784]

Zecca M, Basler K, Struhl G. Direct and long-range action of a wingless morphogen gradient. Cell. 1996; 87:833–844. [PubMed: 8945511]
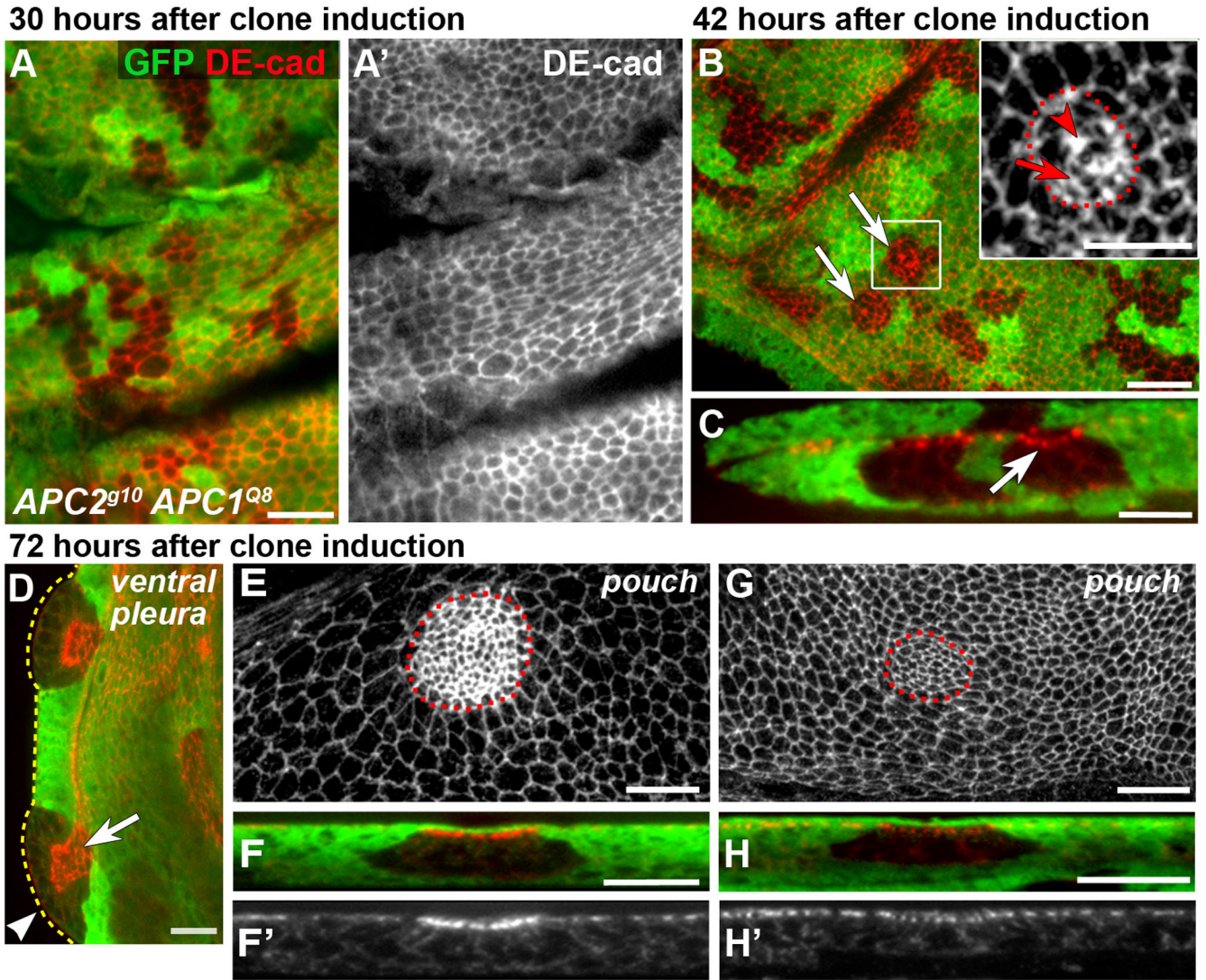
Fig. 1.
APC null clones have smooth borders, apically constrict, invaginate and display elevated DE-cad. No GFP (green) = *APC* null clones. DE-cad (red or grey). Dotted lines indicate clone boundaries (B inset, E, G) or the edge of the disc (D). Larvae were maintained at 21–23°C. (A, A') *APC* null clones 30 hours after clone induction have irregular borders. (B) By 40–42 hours after clone induction, 4% of *APC* null clones have smooth borders (arrows; n = 304 clones, 15 discs). Inset: rectangle in (B). A few mutant cells are apically constricted (arrow) and DE-cad appears increased at multicellular junctions (arrowhead). (C) Cross-section of clone in B showing slight invagination (arrow). (D) *APC* null clones 72 hours after clone induction exhibit smooth borders, apical constriction (arrow indicates adherens junctions [AJs]), and invagination (basal protrusion, arrowhead). (E) Projection of AJs in the pouch with elevated DE-cad in apically constricted cells. (F, F') Cross-section of invaginated clone in E. Projection (G) and cross-section (H, H') of AJs in apically constricted *APC* null cells in the notum without apparent elevated DE-cad. GFP expressing

cells above AJs in (F, H) are peripodial cells. Scale bars: 10 μm in A, B, D–H; 5 μm in B (inset), C.
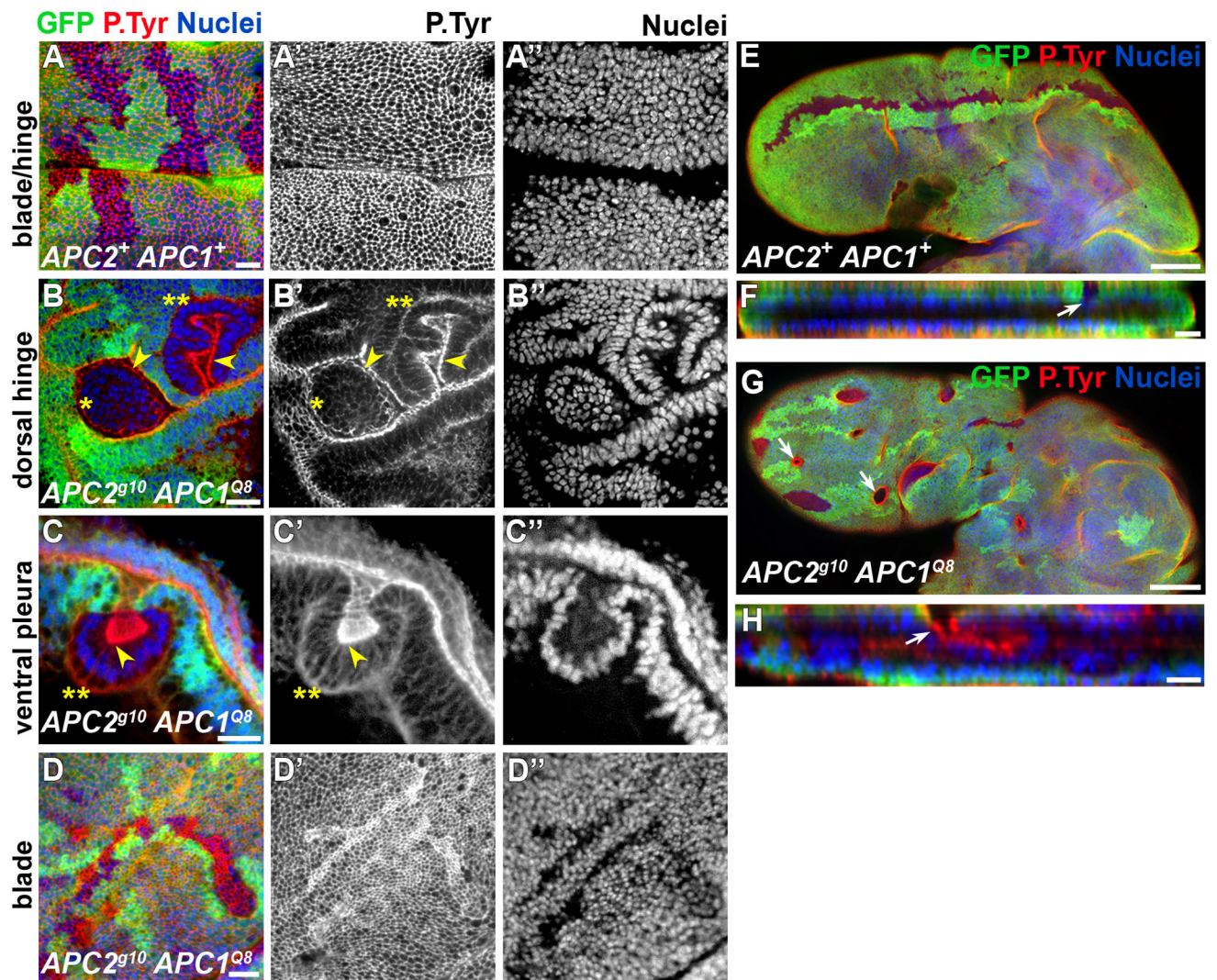
Fig. 2.

APC null clones exhibit position dependent protrusion. Late 3rd larval instar wing discs (A–D"; 96–120 hours after clone induction) and pupal wings (E–H; 6 hours after puparium formation) labeled for GFP (green), phosphotyrosine (red, AJ marker), and propidium iodide (blue, nuclei) as indicated. Absence of GFP = clone. (A–A") Wild type clones have uneven borders and are continuous with the surrounding epithelium. (B–C") The position of AJs (arrowheads) indicates evaginating, apically protruding clones (single asterisks), and invaginating, basally protruding clones (double asterisks) in the dorsal hinge and ventral pleura. Clones in the pouch (D–D") do not significantly invaginate and protrude at this time. (E–H) Pupal wings with wild-type (E, F, arrow) or *APC* null clones (G, H, arrow). Some clones in the blade have invaginated and protrude basally between the developing blades (H, arrow). Scale bars: 10 μm in A–D, F, H; 50 μm in E, G.
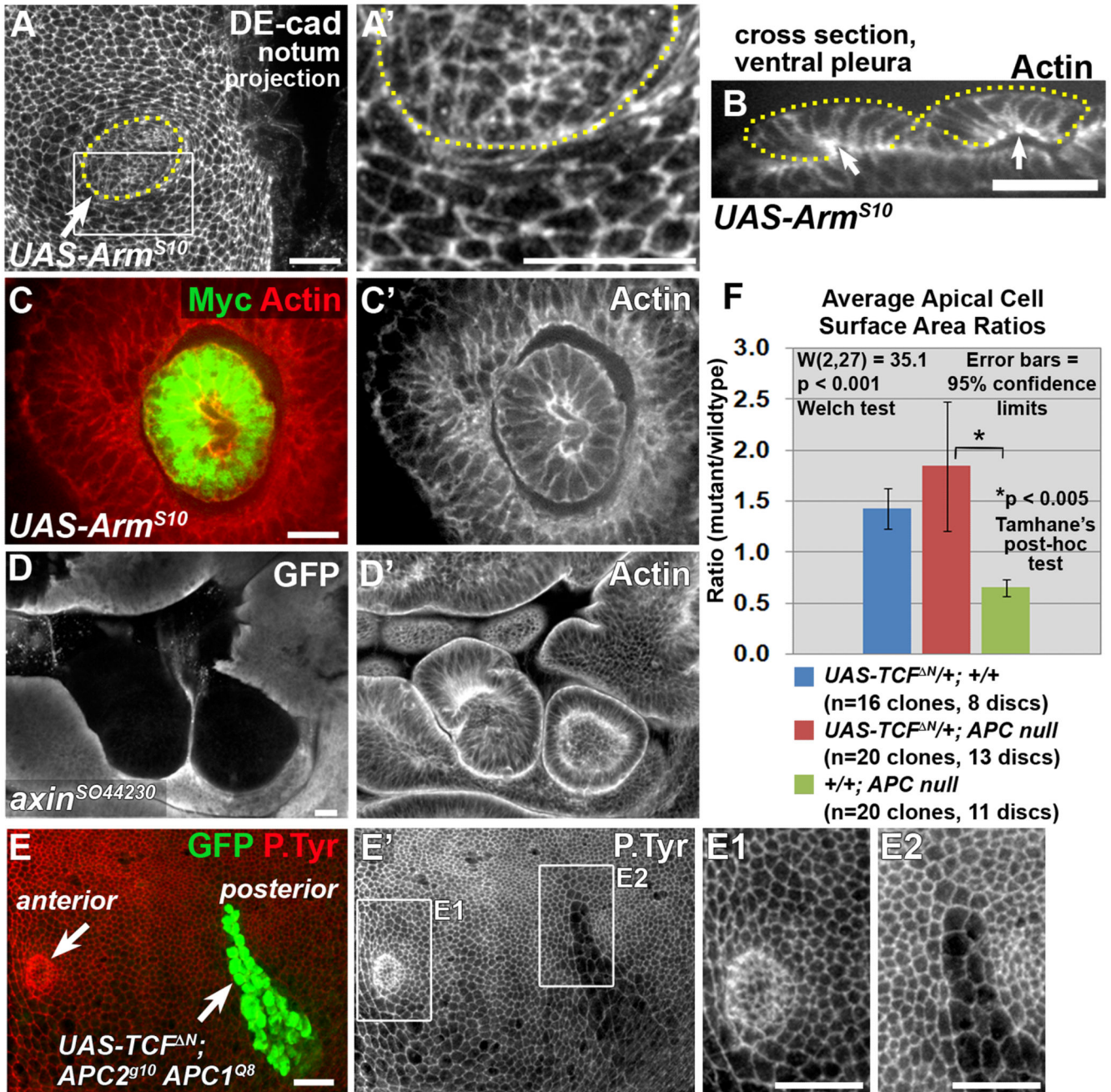
Fig. 3.
Canonical Wnt pathway activation triggers morphological changes in *APC* null clones. Late 3rd larval instar wing discs. Clones expressing stabilized Arm (UAS-Arm^S10-Myc; A–C'), and *axin* null clones (D, D') closely resemble *APC* null clones by exhibiting apical constriction (A, A') invagination/evagination (B, arrows indicate apical surface of invaginated clones; C–D'), and smooth borders (A–D'). Dotted lines indicate clone borders (based on Myc expression). (A') Close-up of the area in the rectangle in A. (E–E2) The *APC* null phenotype is suppressed in *APC* null clones in the posterior compartment expressing TCF ^N and GFP driven by *engrailed-GAL4* using mosaic analysis with a repressible cell

marker (MARCM). While *APC* null clones in the posterior compartment express both GFP and TCF ^{N}, *APC* null clones in the anterior compartment do not express either GFP or TCF ^{N} (E, arrows). In the anterior compartment, clone boundaries were determined by loss of APC2 (not shown). (E1, E2) Close-ups of areas in rectangles in E'. (F) Quantification of average apical cell surface area ratios of indicated genotypes (ratio = average area per cell in clone cells/average area per cell in neighboring cells). Scale bars: 10 µm.
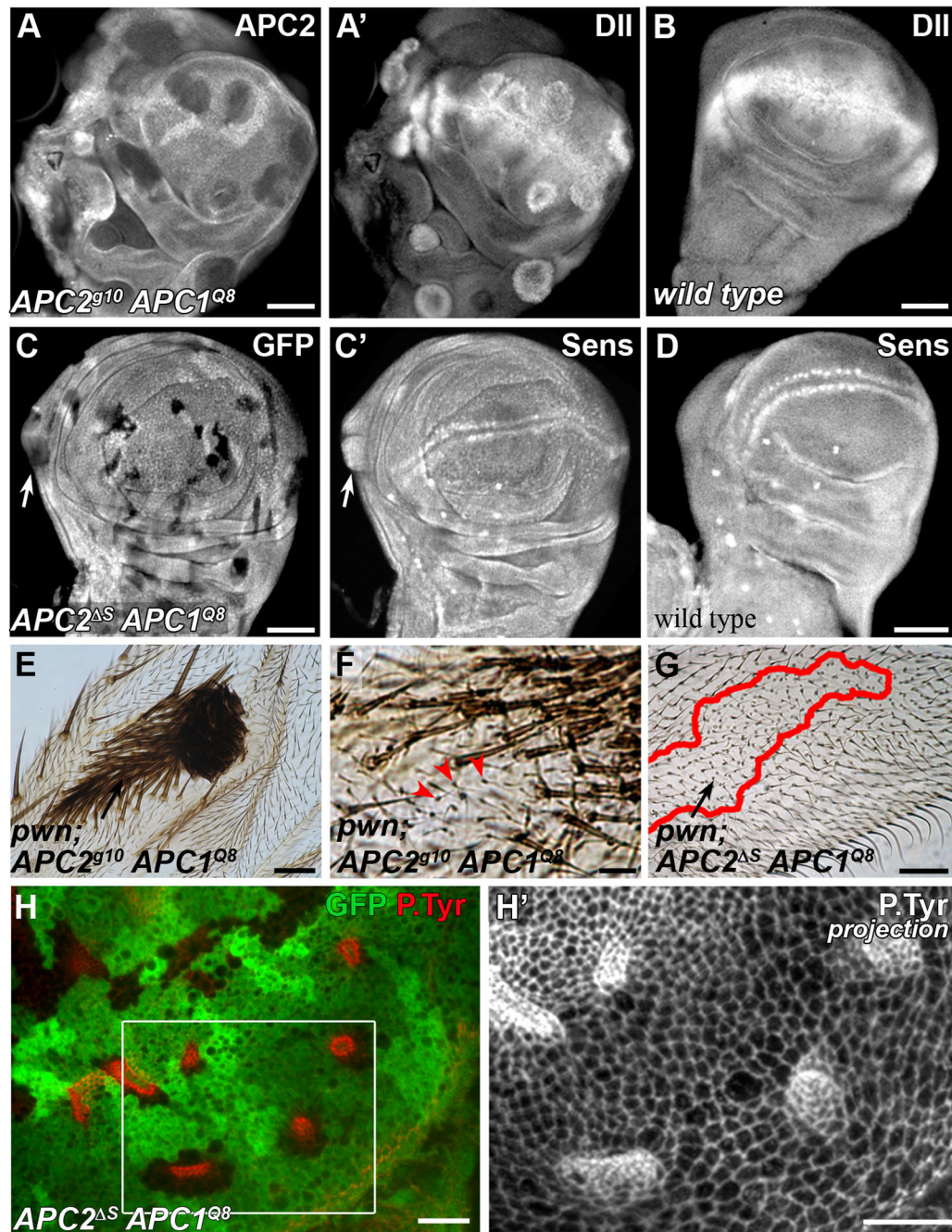
Fig. 4.
Canonical Wnt-dependent cell shape changes can be decoupled from canonical Wnt-dependent cell fate transformation. (A–D) Late 3rd larval instar wing discs. (A, A') Ectopic Dll expression in *APC* null clones, marked by the absence of APC2. (B) Wild type expression of Dll. (C, C') Hypomorphic *APC2 ^{S} APC1^{Q8}* clones occasionally activate Sens (arrow). (D) Wild-type expression of Sens. (E–G) Adult wings *with pawn (pwn)* marked *APC* mutant clones. (E) *pwn; APC2^{g10} APC1^{Q8}* clones develop ectopic margin bristles in the blade. (F) *pwn* marked wing hairs in a *pwn; APC2^{g10} APC1^{Q8}* clone indicate a few cells

that did not undergo the cell fate transformation (arrowheads). (G) *pwn*; *APC2* ^{S} *APC1*^{Q8} clones in the blade (arrow) do not develop margin bristles. Line = clone border. (H) Late 3rd instar wing disc with *APC2* ^{S} *APC1*^{Q8} clones in pouch, marked by absence of GFP. (H') Optical projection of the area in rectangle (H) showing smooth borders and apical constriction in *APC2* ^{S} *APC1*^{Q8} clones occur in the absence of change from blade to margin fate. Scale bars: 50 μm in A–G; 10 μm in H, H'.
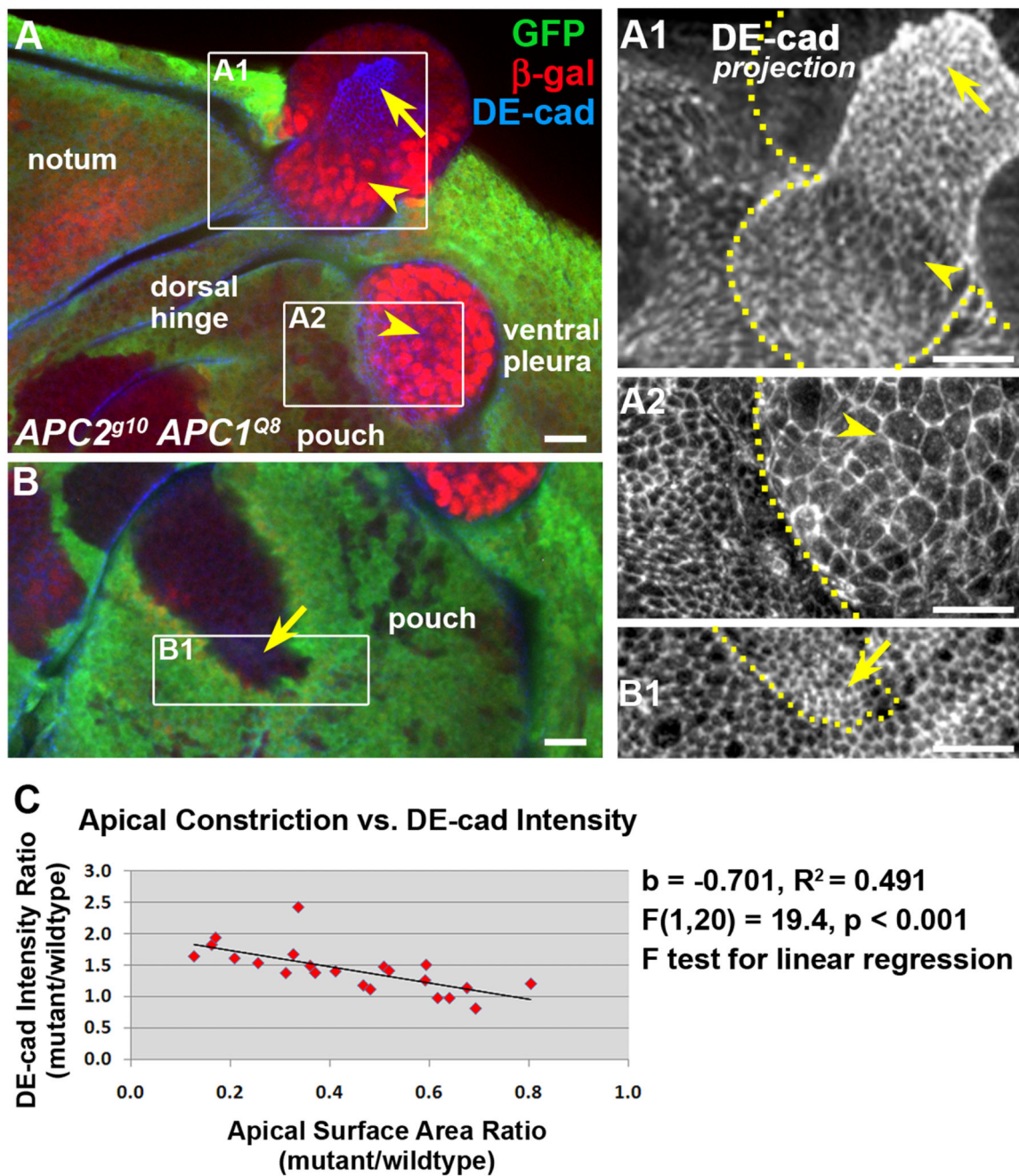
Fig. 5.
DE-cad transcriptional upregulation does not positively correlate with apical constriction in *APC* null cells. Late 3rd larval instar wing discs. Antigens as indicated. *APC* null clones are indicated by the lack of GFP (green). *DE-cad-lacZ* transcriptional reporter activity is detected by immunolocalization of β-galactosidase (red). A1-B1 are projections of DE-cad immunolocalization of areas in rectangles in A, B. Apically constricted cells that lack *DE-cad-lacZ* activity (A, A1, B, B1, arrows). Some *APC* null cells that are not apically constricted activate the *DE-cad-lacZ* reporter (A, A1, A2, arrowheads; n=25 clones). In

some regions of the disc cells appear to apically expand and apically extrude (A, A2, arrowheads). These apically expanded cells robustly activate the *DE-cad-lacZ* reporter. Dotted lines in A1, A2, B1 indicate clone boundaries. (C) Plot of statistically significant correlation between apical constriction and DE-cad pixel intensity. More apical constriction (smaller cell surface area ratio) correlates with higher DE-cad pixel intensity. Scale bars: 10 μm.
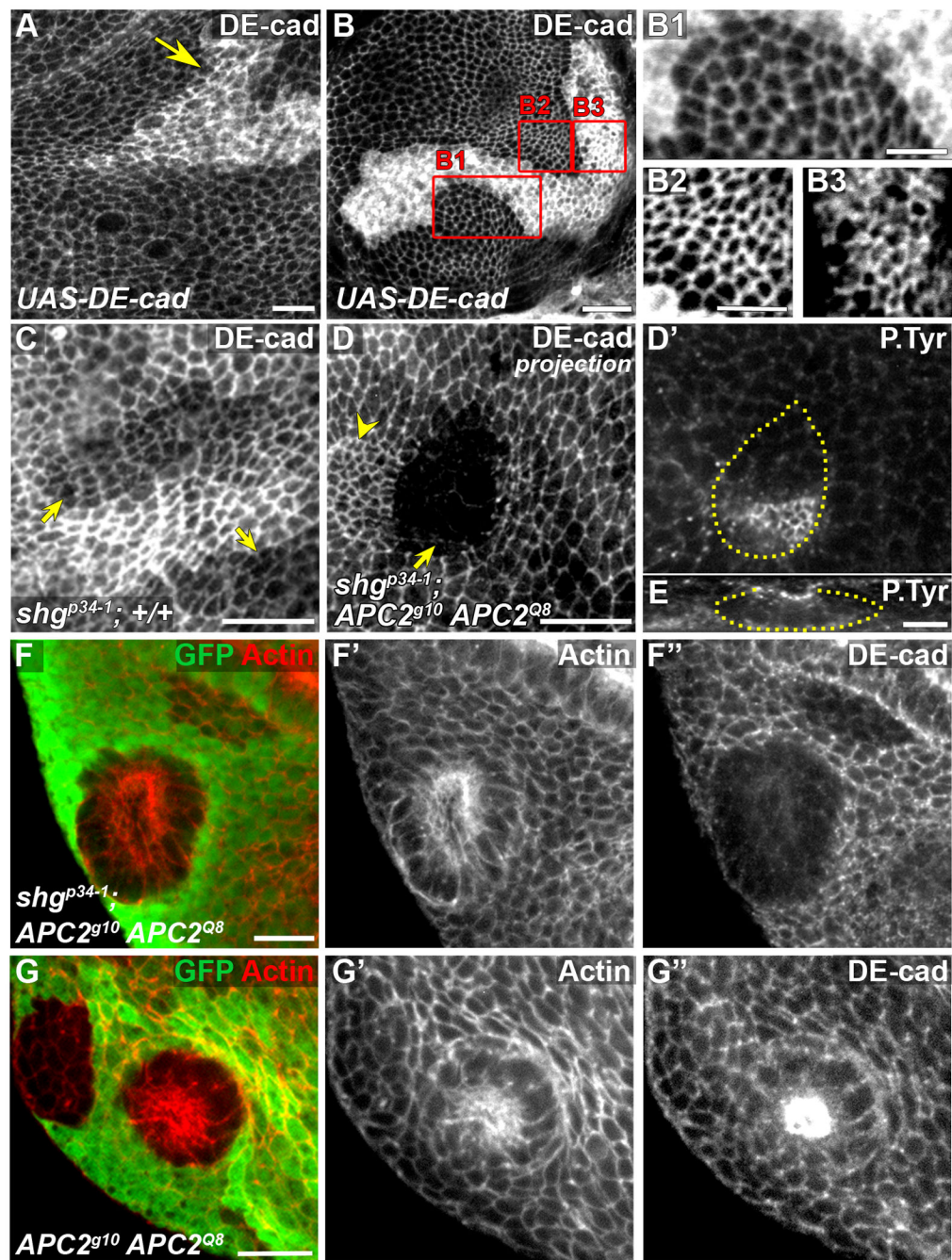
Fig. 6.
Elevated DE-cad is neither necessary nor sufficient for the *APC* null phenotype. Late 3rd larval instar wing discs. (A–B) UAS-DE-cad overexpression using act>CD2>GAL4 FLP-out, marked by elevated DE-cad. *UAS-DE-cad* clones in notum with no apical constriction and exhibiting uneven (A) or smooth (B,B1) borders (arrow). (B2, B3) Close-ups of areas in rectangles B2 and B3 in (B) reveal no difference in apical surface area between cells expressing wild-type levels of DE-cad (B2) and cells expressing elevated DE-cad (B3). Contrast was adjusted in B2 and B3 for comparison. (C) Hypomorphic *shg^{p34-1}* clones

(arrows) have largely normal morphology with reduced levels of DE-cad. (D–E) Apically constricted shg^{p34-1}; $APC2^{g10}$ $APC1^{Q8}$ clone in the wing pouch (arrow). Constricted cells next to the clone (indicated with yellow arrowhead) belong to a neighboring $+/shg^{p34-1}$; $APC2^{g10}$ $APC1^{Q8}$ clone. (D') Phosphotyrosine staining reveals constricted cells that are invaginating (E, cross-section of clone in D'). Plane in D' is at the level of the AJs of the invaginated cells. Clone outline (yellow line) is based on absence of β-galactosidase (not shown) and DE-cad reduction. (F-F") shg^{p34-1}; $APC2^{g10}$ $APC1^{Q8}$ clones basally protrude like $APC2^{g10}APC1^{Q8}$ clones (G–G"). Scale bars: 10 μm in A, B, C–D', F, G; 5 μm in B1-B3, E.
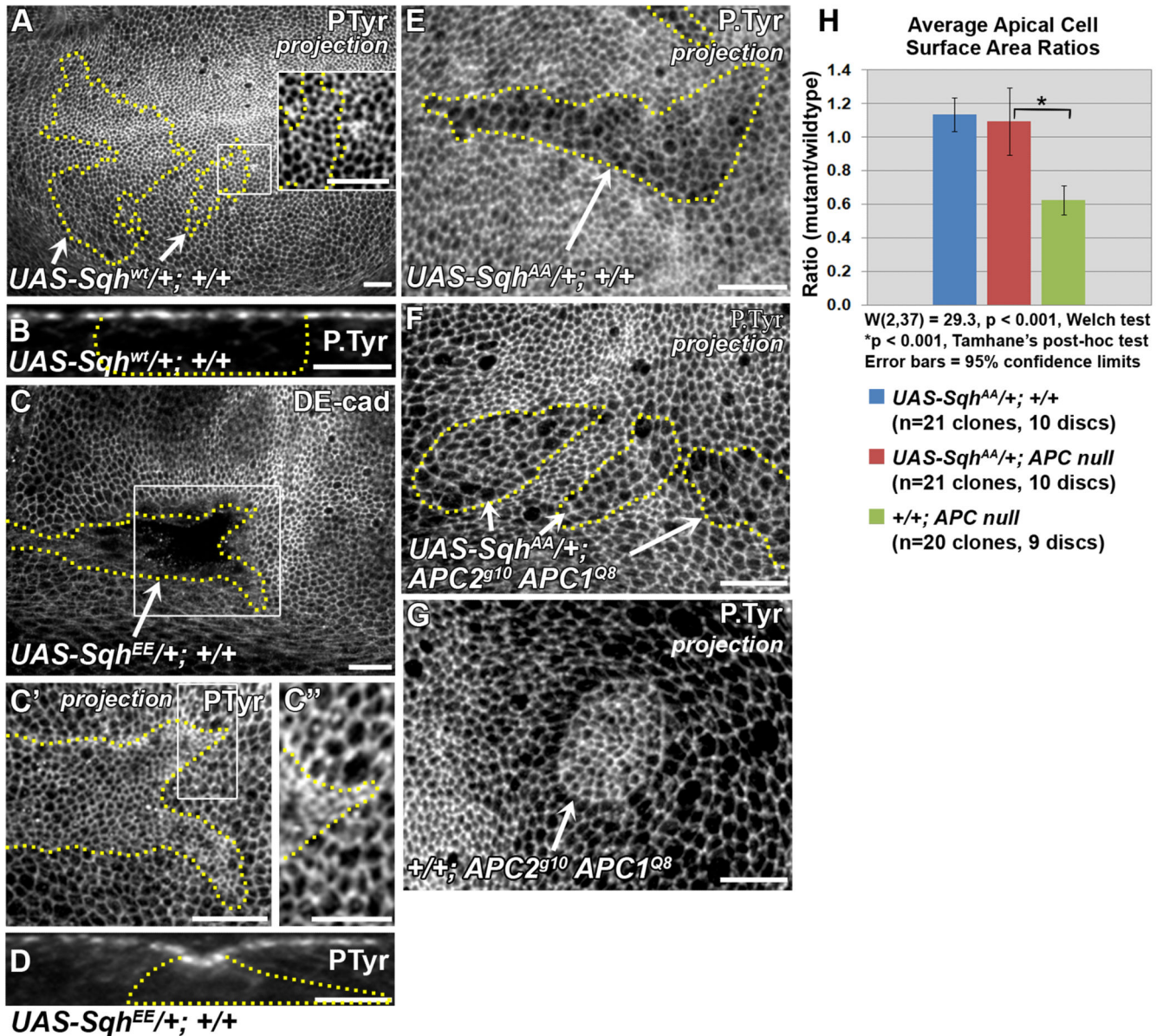
Fig. 7.

Apical constriction of *APC* null clones requires activated Myosin. Late 3rd larval instar wing discs. Yellow lines indicate clone borders. All clones are in the wing pouch. *UAS-Sqh* clones were generated in the posterior compartment using MARCM. (A) *UAS-Sqh*[wt] clones in wing pouch are indistinguishable from wild-type cells. Inset shows close-up of area in rectangle. (B) Cross-section of a *UAS-Sqh*[wt] clone showing lack of invagination. (C) Clone cells overexpressing a phosphomimetic form of Sqh (Sqh[EE]) invaginate. (C') optical projection of area in rectangle in C showing apical constriction. (C'') Close-up of area in rectangle in C'. (D) Cross-section of an invaginated *UAS-Sqh*[EE] clone. (E,H) Expression of non-phosphorylatable Sqh (UAS-Sqh[AA]) in cells wild type for *APC* results in weak apical expansion. (F, H) Apical constriction is suppressed in *APC* null clones expressing Sqh[AA].

(G) Apically constricted *APC* null clone. (H) Comparison of average apical cell surface area ratios in indicated genotypes. Scale bars: 10 μm in A, C, C', E–G; 5 μm in inset in A, B, C", D.
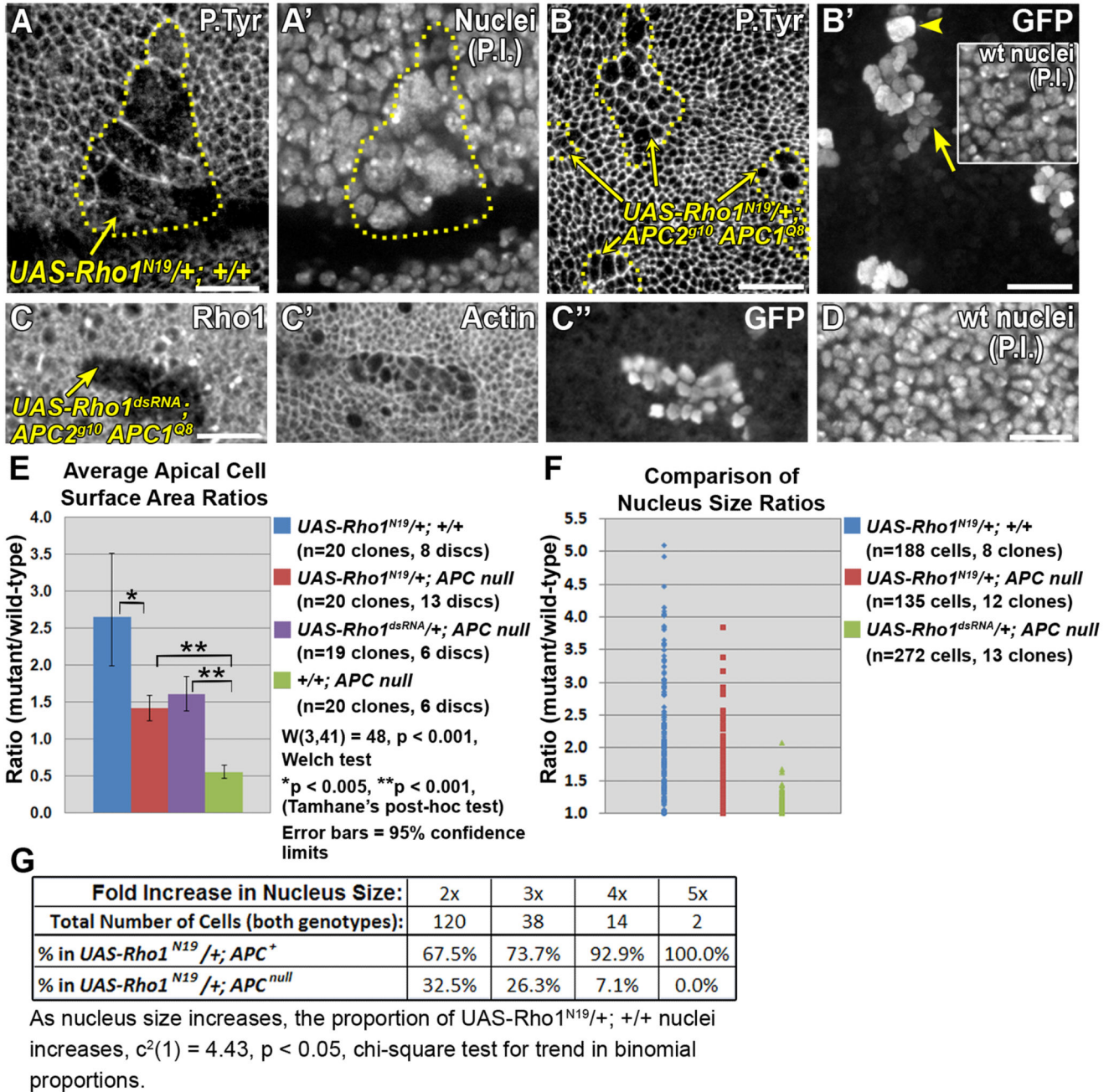
Fig. 8.
Apical constriction in *APC* null clones requires Rho1. Late 3rd larval instar wing discs. (A–B') Larvae were maintained at 18°C after clone induction. (A, A') *UAS-Rho1^{N19}*/+;+/+ clone (driven by *en-GAL4* using MARCM) showing severe apical expansion (A) and abnormally large nuclei [propidium iodide (P.I.)] (A'). Yellow line indicates clone border. (B, B') *APC* null clones expressing *UAS-Rho1^{N19}* display weak apical expansion (B, yellow lines, arrows), and primarily normal sized nuclei (B', arrow, compared with wild type nuclei in inset). Occasional abnormally large nuclei are observed (B', arrowhead). (C–D) Larvae

were maintained at 21–23°C after clone induction. (C-C") *APC* null clone expressing *UAS-Rho1^{dsRNA}*, driven by *en-GAL4* using MARCM, marked by reduced Rho1 (C) and nuclear GFP (C"). Cells are apically expanded (C'), but have normal nucleus sizes compared to wild type nuclei in the same disc location (compare C" with D). (E) Comparison of apical cell surface area ratios in indicated genotypes. (F) Comparison of nucleus size ratios (mutant/wild type as inferred from measuring area, see Methods) in indicated genotypes. (G) Proportion of cells of the indicated genotypes in abnormal nucleus size categories. Statistically significant trend shows proportion of *UAS-Rho1^{N19}*/+; +/+ cells increases as nucleus size increases. Scale bars: 10 μm.

Table 1

Fly stocks	Source/Reference
APC2 alleles	(McCartney et al., 2006)
APC1^{Q8}	(Ahmed et al., 1998)
UAS-Arm^{S10}	(a gift from M. Peifer)
FRT82B axn^{S044230}	(Hamada et al., 1999)
UAS-DE-cadherin	(Sanson et al., 1996)
FRT42B shg^{p34-1}	(Tepass et al., 1996)
UAS-Sqh^{wt}	(Dorsten et al., 2007)
UAS-Sqh^{EE}	(a gift from Franck Pichaud)
UAS-Sqh^{AA}	(Dorsten et al., 2007)
UAS-Rho^{N19}	(a gift from B. Stronach)

All other stocks are from the Bloomington Stock Center or from the Drosophila Genetic Resource Center.

Genotypes used in experiments

y w hsFLP70/+; FRT82B APC2^{g10} APC1^{Q8}/FRT82B Ubi-GFP (or this combination with S, b5, N175K, d40, f90, g41, or e90 alleles of APC2)

y w hsFLP70/+; FRT82B/FRT82B Ubi-GFP

y w hsFLP70/+; pwn; FRT82B Dp(2;3)pwn$^+$/FRT82B APC2^{g10} APC1^{Q8}

y w hsFLP70/+; FRT82B axn^{SO44230}/FRT82B Ubi-GFP

y w hsFLP70/+; UAS-Arm^{S10}/+; act>CD2>GAL4/+

y w hsFLP70/+; UAS-TCF ^{N}/en-GAL4 UAS-GFP; FRT82B APC2^{g10} APC1^{Q8}/FRT82B GAL80

y w hsFLP70/+; UAS-TCF ^{N}/en-GAL4 UAS-GFP; FRT82B/FRT82B GAL80

y w hsFLP70/+; UAS-DE-cadherin/act>CD2>GAL4

y w hsFLP70/+; DE-cadherin-lacZ/+; FRT82B APC2^{g10} APC1^{Q8}/FRT82B Ubi-GFP

y w hsFLP70/+; UAS-DE-shg.DEFL-GFP/act>CD2>GAL4

y w hsFLP70/+; FRT42B shg^{p34-1}/FRT42B GFP^{NLS}; FRT82B APC2^{g10} APC1^{Q8}/FRT82B Ubi-GFP (or FRT82B arm-lacZ)

y w hsFLP70/+: P[APC2$^+$]/+; FRT82B APC2^{g10} APC1^{Q8}/FRT82B Ubi-GFP

y w hsFLP70/+; UAS-Sqh^{wt}/UAS-GFP; act>CD2>GAL4/+

y w hsFLP70/+; UAS-Sqh^{EE}/UAS-GFP; act>CD2>GAL4/+

y w hsFLP70/+; UAS-Sqh^{AA}/en-GAL4 UAS-GFP; FRT82B APC2^{g10} APC1^{Q8}/FRT82B GAL80

y w hsFLP70/+; UAS-Sqh^{AA}/en-GAL4 UAS-GFP; FRT82B/FRT82B GAL80

y w hsFLP70/+;UAS-Rho1^{N19}/en-GAL4 UAS-GFP; FRT82B APC2^{g10} APC1^{Q8}/FRT82B GAL80

y w hsFLP70/+;UAS-Rho1^{N19}/en-GAL4 UAS-GFP; FRT82B/FRT82B GAL80

y w hsFLP70/+;UAS-Rho1^{dsRNA}/en-GAL4 UAS-GFP; FRT82B APC2^{g10} APC1^{Q8}/FRT82B GAL80

Anitbodies/Probes	Dilution	Source
rabbit anti-GFP	1:5000	Abcam
mouse anti-Phosphotyrosine	1:1000	Millipore
rat anti-DE-Cadherin-DCAD2	1:50	Developmental Studies Hybridoma Bank (DSHB)
mouse anti-Rho1	1:50	DSHB

Fly stocks		Source/Reference
mouse anti-CD2	1:2000	DSHB
mouse anti c-Myc	1:50	DSHB
rabbit anti-Distal-less	1:100	S. Carroll (University of Wisconsin)
rabbit anti-Vestigial	1:200	S. Carroll
guinea pig anti-Senseless	1:1000	H. Bellen (Baylor College of Medicine)
rat anti-APC2-CT	1:500	(McCartney et al., 1999)
Alexa 568 phalloidin	1:500	Invitrogen
Propidium Iodide	25 µg/mL	Molecular Probes
mouse anti-β-galactosidase	1:1000	Clontech

Table 2

Disc Compartment	Ratio of Cell Numbers in Clones (non GFP/2x GFP)		*Mutant > Control?
	CONTROL	MUTANT	
Notum	0.98 ± 0.25 (n=11)	1.19 ± 0.43 (n=10)	t=0.966 p = 0.35 df=15
Dorsal Hinge	0.95 ± 0.22 (n=10)	2.47 ± 0.99 (n=10)	Yes t=3.42 p = 0.007 df=10
Pouch	1.25 ± 0.46 (n=9)	1.20 ± 0.39 (n=11)	t=−0.197 p = 0.85 df=17
Ventral Hinge/Pleura	0.97 ± 0.26 (n=7)	1.95 ± 0.39 (n=9)	Yes t=4.96 p = 0.0003 df=13

*Student's t-test, two-tailed, unequal variances